Int. J. Electrochem. Sci., 7 **(2012)** 11264 - 11273

International Journal of
ELECTROCHEMICAL
SCIENCE
www.electrochemsci.org

Phenolic Resin Based Activated Carbon as Cathodes Material for High-Rate Li/$SOCl_2$ Batteries

Shengping Wang[*], *Jian Zeng, Hanyu Zhang, Honggang Zhao, Wei Liu*

Faculty of Material science and Chemistry, China University of Geosciences, Wuhan 430074, PR China
[*]E-mail: robert@cug.edu.cn

Received: 20 September 2012 / *Accepted:* 9 October 2012 / *Published:* 1 November 2012

Activated carbon (PRBAC) was prepared with phenolic resin by the carbonization process and steam activation methods as the cathode materials for high-rate Li/$SOCl_2$ batteries. The electrochemical results show that PRBAC with acetylene black ratio of 60% exhibits high power performance compared with other materials, which is largely attributed to high specific surface area and pore volume and large pore size of PRBAC-60, facilitating an effect adsorption of electrolyte and the diffusion of $SOCl_2$ in the cathode.

Keywords: Activated carbon; Phenolic resin; Li/$SOCl_2$ batteries

1. INTRODUCTION

With the advantages of high energy density, low cost and environmentally friendliness, Li/$SOCl_2$ primary battery, as one of the most important primary batteries, has been widely used with low power consumption applications in civil and military areas [1, 2], for example power supply for land mine and tire pressure monitoring system. However the poor high rate discharge performance prevents their high power output applications, e.g. fish torpedo and civil intellectualized meters. It has been proved that both the electrochemical reaction of Li and the conductivity of electrolyte are suitable for high rate discharge applications. Therefore porous carbon electrodes are the limiting factor for high rate performance in Li/$SOCl_2$ primary batteries. Porous cathodes severs as a catalyst and reaction carrier for the reduction of $SOCl_2$ ($SOCl_2 \rightarrow S + SO_2 + Cl^-$). The indissolvable products (such as S, LiCl [3, 4]) when batteries discharging would deposit on the surface and in the pores of carbon electrode, which will prevent the further reduction reaction of $SOCl_2$ [5, 6]. So the electrochemical performance including high rate performance of Li/$SOCl_2$ primary battery is primarily dependent on the physicochemical properties of carbon materials. The cathode is made of polytetrafluoroethylene

(PTFE) as binder and carbon materials with high specific surface area, abundant porous structure and good conductivity [3, 7, 8]. Acetylene black (AB) is the conventional carbon materials in Li/ $SOCl_2$ primary batteries.

In past decades, a large amount of efforts have been attempted to improve the high rate discharge performance of porous carbon electrodes. An improved high rate discharge performance can be achieved by increasing the effective interface area of cathode in low current density through electrode structural modification. However the energy density of battery is sacrificed to some extent [9]. Additionally, new electrolyte salts (such as $AlCl_3$, $LiAlCl_4$ [8, 10]), additives (such as phthalocyanines metal [11] , porphyrin metal [12], Schiff base [13, 14]) in $LiAlCl_4|SOCl_2$ electrolyte, or conductive additives (such as Cu [15, 16], Pt [17]) in carbon electrode, only show very limited improvements. For its properties, acetylene black made from calcium carbide is only suit for low rate discharging, but not for high rate. It is very necessary to develop appropriate porous carbon material to improve high rate discharge performance. Activated carbon has highly developed internal surface and porous structure compared with acetylene black[18].

In this paper, we attempted to synthesize phenolic resin based activated carbon (PRBAC) by pyrolysis and steam activation the mixture of AB and phenolic resin. Indeed, PRBAC exhibits a remarkably improved high rate discharge capacity in comparison with AB.

2. EXPERIMENTAL

2.1. Samples Preparation

The mixture of AB and phenolic resin was first mechanical ball milled for 1 h and then thermally treated at 800 ^oC for 1 h with a temperature increasing gradient 2 ^oC per minute in a N_2 atmosphere to yield PRBAC. The detailed of PRBAC samples are listed in Table 1. In this paper, sample nomenclature reflects AB ratio in the composite. For example, PRBAC-60 denotes PRBAC with an AB loading of 60%.

Table 1. The detailed of PRBAC samples.

Sample	Acetylene black (wt %)	Phenolic resin (wt %)
PRBAC-0	0	100
PRBAC-20	20	80
PRBAC-40	40	60
PRBAC-60	60	40
PRBAC-80	80	20
PRBAC-100	100	0

2.2. Structural characterization

Structural properties of PRBAC such as surface area, pore volume, and average pore size were investigated from nitrogen adsorption–desorption isotherms using surface area analyzer

(Micromeritics, ASAP2010). The samples were degassed at 300 ^{o}C for 10 h in nitrogen surrounding prior to measuring the properties. The specific surface area was calculated using Brunauer-Emmett-Teller (BET) method. The cumulative pore volume was calculated from the adsorption–desorption profiles. The average pore sizes were estimated by the Joyner-Halenda method.

2.3. Electrochemical test

The composition of the cathodes prepared was 95 wt% PRBAC and 5 wt% PTFE. Six different electrodes were prepared with six PRBAC samples. The cathodes were cast which consisted of spreading slurry of the PBRAC, PTFE and absolute ethanol on a glass plate on both sides of nickel screen (thickness of 50 μm). After cast, the electrodes were detached from the plate and treated at 120 °C for 1 hour and at 240 °C for 20 minutes, that was 37.0 mm×37.0 mm×1.1 mm and their weight except nickel screen was 2.5±0.1g. An electrode with 95 wt% AB and 5 wt% PTFE was prepared with the same procedure and used for comparison.

The AA-size (ER14505) spirally wound test batteries used in the experiments were obtained. The batteries consisted of a carbon cathode (Dried under vacuum at 200 ^{o}C for 24 hour before assembling), lithium anode (37.0 mm×37.0 mm×0.5 mm), and two nonwoven glass fiber mat separators. The assembly is rolled together (anode, separator, cathode, and then separator), and the roll is inserted into a stainless steel battery can with a prewelded burst disk in the base. The battery can is equipped with a stainless steel header assembly with prewelded nickel tabs for the Li anode. The ER14505 test batteries were filled in an Ar filled glove box with 28 mL of electrolyte consisting of 1.5 mol·L^{-1} $LiAlCl_4$ in $SOCl_2$.

The capacities of the ER14505 test batteries at 25 ^{o}C were obtained that the batteries were discharged at 10 mA and 100 mA with 2.0 V cutoff voltage using a model BT2000 Arbin battery test equipment. Multiple experiments were conducted for the same conditions, and the data reported in this work are an average of three or more experiments. The test batteries with different depth of discharge (DOD) were obtained on 10 mA, their cutoff voltages were 3.3 V and 2.5 V, respectively.

Cyclic voltammetry (CV) before discharging and electrochemical impedance spectra (EIS) at different DOD, for instance the open circuit potential (OCP), 3.3 V and 2.5V, were measured on ER14505 test batteries using the VMP3 electrochemical workstation. The carbon cathode in ER14505 was as a work electrode, and the lithium anode was as a reference electrode and auxiliary electrode. The scanning rates of CV were 0.25, 0.75 and 1.00 mV·s^{-1} between 4.0 V and 1.0 V, and frequencies range of EIS were from 10^5 to 10^{-2} Hz with amplitude of 5 mV.

3. RESULTS AND DISCUSSION

3.1. Structural characterization Analysis

The nitrogen adsorption-desorption isotherms of PRBAC and AB display a typical IV curve shown in Fig.1 [19], indicating that these carbons are also microporous. This originated from the

carbonization process of the phenolic resin and should be localized inside the powdered activated carbon and/or in the spacers that connect the powdered activated carbon.

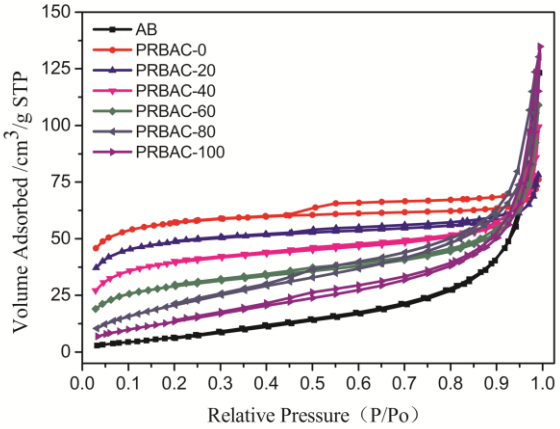

Figure 1. The nitrogen sorption isotherms of PRBAC and AB.

The BET specific surface area, pore volume and average pore diameter were summarized in Table 2. The BET specific surface area (S_{BET}) and pore volume of PBRAC samples decreases with the increase content of AB, while the pore size increases. The PRBAC-60 shows a BET specific surface area of 243.67 $m^2 \cdot g^{-1}$ and a specific pore volume of 2.329 $cm^3 \cdot g^{-1}$ with an average pore diameter of 3.848 nm, which facilitates an effect adsorption of electrolyte and the diffusion of $SOCl_2$ within the porous carbon cathode compared with other PRBAC. Therefore, it is demonstrated that PRBAC-60 exhibits superior electrochemical performance.

Table 2. Performances of PRBAC and AB.

Sample	Physicochemical properties			Reduction kinetic parameters of electrodes		Capacity of ER14505	
	S_{BET} ($m^2 \cdot g$)	average pore diameter (nm)	Pore volume ($cm^3 \cdot g$)	k^0 (cm·s)	D_0 ($cm^2 \cdot s$)	10 mA (mAh)	100 mA (mAh)
PRBAC-0	633.67	2.039	3.229	6.27×10^{-10}	5.03×10^{-7}	1836	503
PRBAC-20	474.94	2.228	2.862	2.99×10^{-9}	2.68×10^{-6}	1900	790
PRBAC-40	384.26	2.979	2.645	2.52×10^{-5}	4.69×10^{-5}	2003	1390
PRBAC-60	243.67	3.848	2.329	4.30×10^{-4}	2.01×10^{-4}	2108	1529
PRBAC-80	156.84	6.082	2.315	1.23×10^{-4}	1.53×10^{-4}	2080	1456
PRBAC-100	102.29	9.106	2.314	9.13×10^{-5}	1.63×10^{-4}	1948	1377
AB	90.20	10.952	2.512	7.55×10^{-5}	1.51×10^{-4}	2005	1394

As has been previously shown, the amount of microporosity depends on the phenolic resin used in the carbonization step and on the temperature and conditions at which the syntheses were performed. BET specific surface area, specific pore volume, and average pore diameter of AB were 90 $m^2 \cdot g^{-1}$, 10.952 $cm^3 \cdot g^{-1}$, and 2.512 nm, respectively.

3.2. Cyclic Voltammetry Analysis

CV curves of PBRAC and AB with different scanning rates are illustrated in Fig.2. There is only one main reduction peak without oxidation peaks detected [14, 20]. PBRAC-0 and PBRAC-20 exhibit positive CV reduction peaks positions and low CV peaks current compared with other PRBAC at different scanning rates. It is supposed that high content of phenolic resin with cross-linking three-dimensional network formed at the carbonization process in PBRAC-0 and PBRAC-20, covering catalytic sites of activated carbon, which accounts for the phenomenon [21]. Furthermore, a less significantly reduction peak at 2.0 V is observed in the CV curves of PBRAC-0 and PBRAC-20, which is ascribed to the reduction of SO_2, associating with the electrode surface [22].

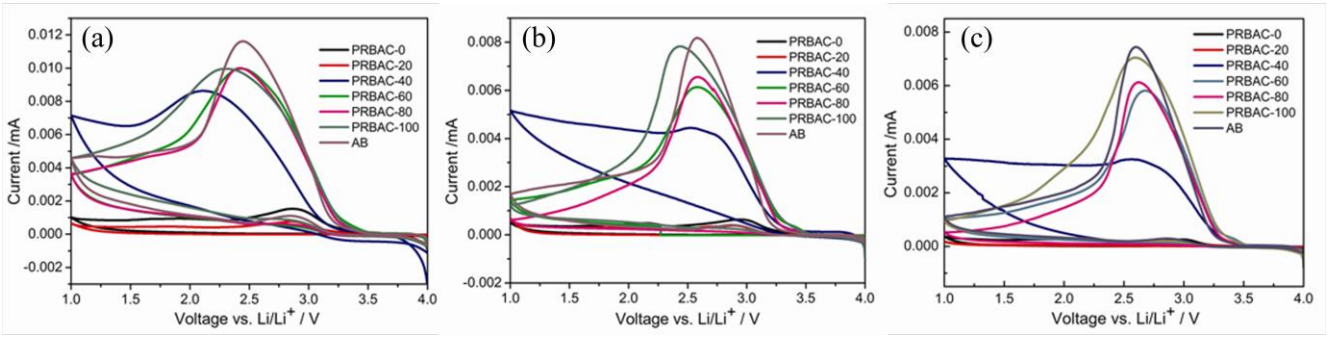

Figure 2. Cyclic voltammograms of PBRAC and AB with 0.00075V/s (a), 0.001V/s (b) and 0.0025V/s (c).

CV reduction peaks positions are shift to positive with increasing scan rates. The relationships of peak current i_p and peak voltage E_p with scan rates $v^{1/2}$ are listed as follows:

$$i_p = (2.99 \times 10^5) n (n_\alpha)^{1/2} A C_0^* D_0^{1/2} v^{1/2} \quad (1)$$

$$i_p = 0.227 nFAC_0^* k^0 \exp[-(^{n_\alpha F}/_{RT})(E_p - E^{0'})] \quad (2)$$

Where n represents the number of electrons transferred, A is the specific area of electrode, C_0^* denotes the bulk concentration of active material, n_α is the apparent number of electrons transferred, D_0 represents the diffusion coefficient of active material, k^0 denotes the constant exchange rate and $E^{0'}$ is the standard electrode potential (3.74V). The relationships of peak current i_p with scan rates

$v^{1/2}$ corresponding to Eq.1, indicate that the reduction of $SOCl_2$ is greatly influenced by diffusion of the active material [23]. Kinetic parameters calculated from Eq.1-2 are given in table 2.

The D_0 and k^0 exhibits upward trends from PRBAC-0 to PRBAC-100, AB. The D_0 of PRBAC-0 and PRBAC-20 is 5.03×10^{-7} $cm^2\cdot s$ and 2.68×10^{-6} $cm^2\cdot s$ respectively, which is far less than the D_0 of other samples. The D_0 of PRBAC-60, PRBAC-80, PRBAC-100 and AB range from 2.01×10^{-4} $cm^2\cdot s$ to 1.51×10^{-4} $cm^2\cdot s$, meaning that the diffusion of $SOCl_2$ occurs in liquid phase [24]. It is supposed that the four samples exhibit larger pore size due to high content of AB, which facilitates an effect adsorption of electrolyte and the diffusion of $SOCl_2$, enabling electrochemical reaction of active material to participate in completely. In contrast, PRBAC-0 and PRBAC-20 exhibit small pore size, which is ascribed to dense colloid formed by un-carbonized phenolic resin, hindering the diffusion and charge transfer of active material. The constant exchange rate k^0 reflects a characteristic value of electron transfer process which is accompanied by the reduction of $SOCl_2$. The low k^0 of PRBAC-0 and PRBAC-20 indicate that dense colloid structure obstructs the reduction of $SOCl_2$ seriously, leading to serious electrochemical polarization at high rate, which correspond with the galvanostatic discharge tests. Especially, the D_0 and k^0 of PRBAC-60 is larger than other samples, indicating that PRBAC-60 possesses a superior electrochemical performance.

3.3. Discharging capacity

Fig.3 shows the galvanostatic discharge profiles of PRBAC and AB as cathode materials for $Li/SOCl_2$ battery. These materials exhibit similar voltage plateau ca. 3.55 V at 10 mA, while voltage plateaus of these materials decrease at 100 mA. PBRAC-0 and PBRAC-20 show low voltage plateaus of 3.4 V. However, PBRAC-60, PBRAC-80, PBRAC-100 and AB possess high plateaus of 3.45 V.

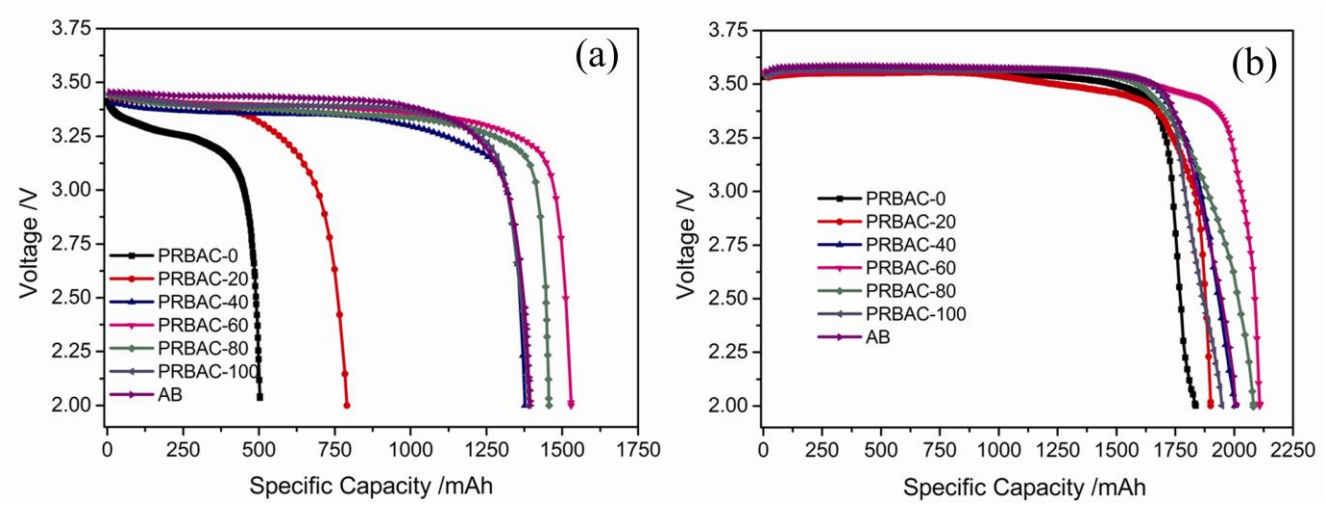

Figure 3. Discharge curves of ER14505 testing batteries at 10 mA (a) and 100 mA (b) with PBRAC and AB as cathodes.

The capacities of ER14505 test batteries with PBRAC and AB at 10 mA are from 1836 mAh to 2108 mAh (in Table 2), but not wide. However, the capacities of batteries with these materials exhibit significant difference at 100mA. PBRAC-0 delivers only 503 mAh, which is far less than the capacity of 2108.1 mAh at 10mA. Because PBRAC-0 presents small active specific surface area among these materials owing to dense morphology structure, formed by the mixture of activated carbon and un-carbonized phenolic resin, which causes catalytic sites of active material to decrease. Furthermore, the micropores of PRBAC-0 can be blocked by the solid discharge products (S and LiCl) with high power output, which prevents the further reduction of $SOCl_2$. In contrast, AB shows a discharge capacity of 1394 mAh, which is attributed to mesopores of AB, facilitating transportation of discharge products and Li ion. It is most prominent that PBRAC-60 delivers the highest discharge capacity of 1529 mAh at 100 mA. Because PBRAC-60 exhibits excellent electrical conductivity and superior catalytic performance with optimal BET specific surface area, pore volume and average pore diameter (Table 2), which preserves transport of Li ion to the active material and enables electrochemical reaction of $SOCl_2$ participate in completely. Therefore, PBRAC-60 obtains the superior electrochemical performance for high-rate Li/$SOCl_2$ battery.

3.4. EIS

The EIS for PRBAC and AB at different DOD are shown in Fig.4. All impedance spectra show a semicircle at high frequencies corresponding to the solid electrolyte membrane (SEI) of electrode surface and a short inclined line in low frequency due to the ion diffusion within the cathode at OCP. It is noted that the beginning of arc is below 0, ascribed to the presence of electrical inductance in equivalent circuit, which may be related to the porosity of carbon cathode [25], and yields little influence for electrochemical performance of circuit.

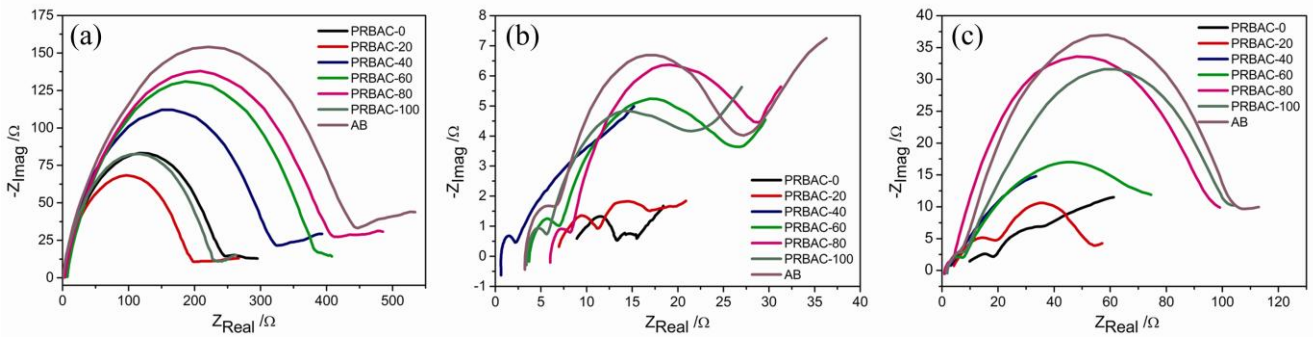

Figure 4. Ac impedance spectra of PBRAC and AB at OCP (a), 3.3V (b) and2.5V (c).

When discharged to 3.3 V, the impedance spectra of all materials exhibit two depressed semicircles in high frequency region and in middle frequency region followed by a short inclined line in low frequency region. The depressed semicircles in high frequency region at the depth of discharge of 3.3 V are smaller than the arc at OCP. It is assumed that two depressed semicircles in high

frequency region and in middle frequency region reflect the presence of discharge product LiCl, accompanying by the disappearance of SEI layer of carbon electrode. Generally, LiCl layer is constituted by the compact layer and porous layer [26]. The compact layer prevents good electrolyte penetration of the active material due to the dense morphology structure, possessing excellent electrical conductivity, while porous layer facilitates the transportation of Li ions to the active material [6]. However, porous LiCl layer formed at initial discharge state hinders the diffusion of $SOCl_2$ and Li ions. Therefore, the impedance spectra in low frequency region shows inclined line, indicating a character of diffusion in solid phase. LiCl layer on electrode surface becomes dense gradually with increase of the depth of discharge, preventing the diffusion of Li ions seriously. And slightly inclined lines become depressed semicircle gradually with the increase of the resistance of LiCl layer due to the dense LiCl layer. The diameter of two depressed semicircles in high frequency region and in middle frequency region becomes large, meaning that the resistance of compact layer and porous layer increases. Especially, the depressed semicircle in middle frequency region increasing dramatically indicates the rapid growth of compact layer during discharge process. The inclined line in low frequency region reflects the charge transfer of reduction of $SOCl_2$ between carbon electrode and electrolyte. The angles of inclined lines of these materials is slightly above 45° at initial state of discharge, while the angles of these inclined lines decreases to 45° with the increase of depth of discharge. It is assumed that the phenomenon is caused by the liquid phase diffusion of $SOCl_2$ at initial state of discharge and the presence of double layer capacitance.

The angles of inclined lines of PRBAC-0 and PRBAC-20 increase slightly at the end state of discharge. However, the inclined lines of PRBAC-60, PRBAC-80, PRBAC-100 and AB disappear suddenly at the depth of discharge of 2.0 V. Because LiCl layer on electrode surface becomes dense gradually with increase of the depth of discharge, and compact layer forms at the end state of discharge, causing the resistance of the LiCl layer to increase. Thus the angles of inclined lines of PRBAC-0 and PRBAC-20 increase slightly at the end state of discharge attributed to micropores of PRBAC-0 and PRBAC-20. However, the structure of PRBAC-60, PRBAC-80 and PRBAC-100 is different from PRBAC-0 and PRBAC-20, which changes the time constant of RC circuit. As a result, the inclined lines of PRBAC-60, PRBAC-80 and PRBAC-100 can not be revealed over frequency range. Therefore, the trend of LiCl layer on electrode surface becomes dense gradually with increase of the depth of discharge is proven by the changes of the inclined lines in low frequency region. According to the trend, it is conclusion that the rate-controlling step of reduction of $SOCl_2$ varies from diffusion of $SOCl_2$ between carbon electrode and electrolyte to diffusion of $SOCl_2$ through porous layer of LiCl layer [27].

4. CONCLUSIONS

In summary, phenolic resin based activated carbon was prepared by the carbonization process and steam activation methods as the cathode materials for high-rate Li/$SOCl_2$ batteries, using phenolic resin and acetylene black as raw materials. The BET tests results indicate that PRBAC-60 shows high specific surface area and pore volume and large pore size, which facilitates an effect adsorption of

electrolyte and the diffusion of $SOCl_2$ within the cathode. The PRBAC-60 delivers the highest discharge capacity of 1529 mAh with current of 100mA, due to the excellent electrical conductivity and superior catalytic performance of phenolic resin-based activated carbon and mesopores of AB. The CV results are also proven that PBRAC-60 exhibits the optimal electrochemical performance for high-rate Li/$SOCl_2$ battery. Furthermore, it is conclusion that the rate-controlling step of reduction of $SOCl_2$ is the diffusion of $SOCl_2$ through porous layer of LiCl layer.

ACKNOWLEDGEMENTS
This work was financially supported by the Key Program of Natural Science Foundation of Hubei Province, China (2010CDA017).

References

1. J. J. Auborn, K. W. French, S. I. Lieberman, V. K. Shah and A. Heller, *J. Electrochem. Soc.*, 120 (1973) 1613-1619.
2. W. K. Behl, J. A. Christopulos, M. Ramirez and S. Gilman, *J. Electrochem. Soc.*, 120 (1973) 1619-1623.
3. A. N. Dey, J. S. Miller and W. L. Bowden, *US Patent* 4177329 (1979).
4. A. N. Dey, *J. Electrochem. Soc.*, 123 (1976) 1262-1264.
5. A. N. Dey and P. Bro, *J. Electrochem. Soc.*, 125 (1978) 1574-1578.
6. Y. L. Zhang and C. S. Cha, *Electrochim. Acta*, 37 (1992) 1207-1210.
7. K. M. Abraham, L. Pitts and W. P. Kilroy, *J. Electrochem. Soc.*, 132 (1985) 2301-2308.
8. K. A. Klinedinst and M. J. Domeniconi, *J. Electrochem. Soc.*, 127 (1980) 539-544.
9. M. Jain, G. Nagasubramanian, R. G. Jungst and J. W. Weidnera, *J. Electrochem. Soc.*, 146 (1999) 4023-4030.
10. J. G. Chiu, Y. Y. Wang and C. C. Wan, *J. Power Sources*, 21 (1987) 119-131.
11. Z. W. Xu, J. S. Zhao, H. J. Li, K. Z. Li, Z. Y. Cao and J. H. Lu, *J. Power Sources*, 194 (2009) 1081-1084.
12. O. A. Baturina, L. S. Kanevsky, V. S. Bagotzky, V. V. Volod'ko, A. L. Karasev and A. A. Revina, *J. Power Sources*, 36 (1991) 127-136.
13. W. S. Kim, W. J. Sim, K. I. Chung, Y. E. Sung and Y. K. Choi, *J. Power Sources*, 112 (2002) 76-84.
14. W. S. Kim and Y. K. Choi, *Appl. Catal., A*, 252 (2003) 163–172.
15. V. G. Danilov and V. I. Shilkin, *J. Power Sources*, 45 (1993) 7-13.
16. S. Szpak and J. R. Driscoll, *J. Power Sources*, 10 (1983) 343-354.
17. K. A. Klinedinst, *J. Electrochem. Soc.*, 128 (1999) 2507-2512.
18. G. Hasegawa, K. Kanamori, K. Nakanishi and T. Hanada, *Carbon*, 48 (2010) 1757-1766.
19. B. V. Kaluđerović, L. Kljajević, D. Sekulić, J. Stašić and Ž. Bogdanov, *Chem. Ind. Chem. Eng. Q.*, 15 (2009) 29-31.
20. Y. K. Choi, B. S. Kim and S. M. Park, *J. Electrochem. Soc.*, 140 (1993) 11-18.
21. B. G. Li, H. B. Liu, L. Zhang, Y. D. He and H. B. Zhang, *Carbon* (in Chinese), 04 (2004) 15-19.
22. M. J. Madou, J. J. Smith and S. Szpak, *J. Electrochem. Soc.*, 134 (1987) 2794-2798.
23. W. S. Kim, K. Chung, S. K. Kim, S. Jeon, Y. H. Kim, Y. E. Sung and Y. K. Choi, *Bull. Korean Chem. Soc.*, 21 (2000) 571-576.
24. C. O. Bennett and J. E. Myers, *Momentum, heat, and mass transfer*, McGraw-Hill, New York, USA(1962).

25. H. H. Ge, Y. S. Guo, R. F. Guo, Y. P. Wu and G. D. Zhou, *J. Appl. Electrochem.*, 39 (2009) 155-158.
26. M. Aubay and E. Lojou, *J. Electrochem. Soc.*, 141 (1994) 865-872.
27. S. B. Lee, S. I. Pyun and E. J. Lee, *Electrochim. Acta*, 47 (2001) 855-864.